

Ground state solution of Bose-Einstein condensate by directly minimizing the energy functional

Weizhu Bao *

Department of Computational Science
National University of Singapore, Singapore 117543.

Weijun Tang †

Department of Computational Science,
National University of Singapore, Singapore 117543
and Institute of Applied Physics and Computational Mathematics
P.O. Box 8009, Beijing, 100088, P.R. China.

Abstract

In this paper, we propose a new numerical method to compute the ground state solution of trapped interacting Bose-Einstein condensation (BEC) at zero or very low temperature by directly minimizing the energy functional via finite element approximation. As preparatory steps we begin with the 3d Gross-Pitaevskii equation (GPE), scale it to get a three-parameter model and show how to reduce it to 2d and 1d GPEs. The ground state solution is formulated by minimizing the energy functional under a constraint, which is discretized by the finite element method. The finite element approximation for 1d, 2d with radial symmetry and 3d with spherical symmetry and cylindrical symmetry are presented in detail and approximate ground state solutions, which are used as initial guess in our practical numerical computation of the minimization problem, of the GPE in two extreme regimes: very weak interactions and strong repulsive interactions are provided. Numerical results in 1d, 2d with radial symmetry and 3d with spherical symmetry and cylindrical symmetry for atoms ranging up to millions in the condensation are reported to demonstrate the novel numerical method. Furthermore, comparisons between the ground state solutions and their Thomas-Fermi approximations are also reported. Extension of the numerical method to compute the excited states of GPE is also presented.

*Email address: bao@cz3.nus.edu.sg. Fax: 65-67746756

†Email address: tang_tangwj@yahoo.com.

Key Words: Bose-Einstein condensation (BEC), ground state solution, Gross-Pitaevskii equation (GPE), energy functional, finite element approximation, Thomas-Fermi approximation.

1 Introduction

Recently, there have been experiments of Bose-Einstein condensation (BEC) in dilute bosonic atoms (alkali and hydrogen atoms) employing magnetic traps at ultra-low temperatures [7, 13, 23]. The condensation can consist of few thousand to millions of atoms confined by the trap potential. This peculiar state of matter, whose existence was postulated back in the 1920s by Bose [12] and Einstein [22], exhibits several characteristics which set it apart from other homogeneous condensed matter systems [30, 18]. In fact, besides internal interactions, the macroscopic behavior of BEC matter is highly sensitive to the shape of the external trapping potential. Theoretical predictions of the properties of BEC matter can now be compared with experimental data by adjusting some tunable external parameters, such as the trap frequency and/or aspect ratio. Needless to say, these dramatic progresses on the experimental front are stimulation a corresponding wave of activity on both the theoretical and the numerical fronts.

The properties of a BEC at temperatures T very much smaller than the critical temperature T_c [30, 25] are usually described by the nonlinear Schrödinger equation (NLSE) for the macroscopic wave function known as the Gross-Pitaevskii equation (GPE) [27, 36]. Note that equations very similar to the GPE also appear in nonlinear optics where an index of refraction which depends on the light intensity leads to a nonlinear term like the one encountered in the GPE.

There has been a series of recent studies which deal with the numerical solution of the time-independent GPE for ground state and the time-dependent GPE for finding the dynamics of a BEC. For numerical solution of time-dependent GPE, Bao et al. [9, 10, 11] presented a time-splitting spectral method, Ruprecht et al. [37] and Adhikari et al. [4, 5] used the Crank-Nicolson finite difference method to compute the ground state solution and dynamics of GPE, Cerimele et. al. [15] proposed a particle-inspired scheme. For ground state solution of GPE, Edwards et al. [21] presented a Runge-Kutta type method and used it to solve 1d and 3d with spherical symmetry time-independent GPE. Adhikari [2, 3] used this approach to get the ground state solution of GPE in 2d with radial symmetry. Other approaches include an explicit imaginary-time algorithm used by Cerimele et al. [14] and Chiofalo et al. [16], a direct inversion in the iterated subspace (DIIS) used by Schneider et al. [38], and a simple analytical type method proposed by Dodd [20].

In this paper, we propose a new numerical method to compute the ground state solution of Bose-Einstein condensation by directly minimizing the energy functional through the finite element discretization. We begin with the 3d Gross-Pitaevskii equation, make it dimensionless to obtain a three-parameter model, show how to approximately reduce it to a 2d GPE and a 1d GPE in certain limits. The ground

state solution is formulated by directly minimizing the energy functional under a constraint. Furthermore we present in detail the finite element approximation of the minimization problem for 1d, 2d with radial symmetry and 3d with spherical symmetry and cylindrical symmetry (this is the most popular case in the current experiments of BEC), and provide approximate ground state solutions, which are used as initial guess in our practical numerical computation, in two extreme regimes: very weak interactions and strong repulsive interactions. Numerical results in 1d, 2d with radial symmetry and 3d with spherical symmetry and cylindrical symmetry for atoms ranging up to millions in the condensation are reported to demonstrate the numerical method. Furthermore, comparisons between the ground state solutions and their Thomas-Fermi approximations are also reported by using our numerical method. Our numerical results show that the Thomas-Fermi approximation is a ‘good’ approximation to the ground state solution in the strong repulsive interaction regime, but a ‘worse’ approximation in the medium interaction regime. Convergence rate of the Thomas-Fermi approximation to the ground state solution as a function of the number of atoms in the condensation is also reported by our method. Furthermore, we also extend our method to compute the excited states of GPE in 1d.

The paper is organized as follows. In Section 2 we begin with the 3d GPE, scale it to get a three-parameter model, show how to reduce it to lower dimensions. In Section 3 we present a new method to compute the ground state solution of a BEC by directly minimizing the energy functional and provide the approximate ground state solution in two extreme regimes: very weak interactions and strong repulsive interactions. In Section 4 we present detailed numerical formula and its finite element approximation for the ground state solution of GPE in 1d, 2d with radial symmetry and 3d with spherical symmetry (in these cases, it is reduced to a 1d problem), and in section 5 for 3d with cylindrical symmetry (in this case, it is reduced to a 2d problem). In Section 6 we report on numerical results of the ground state solution of BEC in 1d, 2d with radial symmetry and 3d with spherical symmetry as well as cylindrical symmetry. In Section 7 some conclusions are drawn.

2 Gross-Pitaevskii equation

In this section, we will present the Gross-Pitaevskii equation in three dimension, how to scale it to a three-parameter model and reduction to lower dimension.

At zero or very low temperature, a BEC is well described by the macroscopic wave function $\psi(\mathbf{x}, t)$ whose evolution is governed by a self-consistent, mean field nonlinear Schrödinger equation known as the Gross-Pitaevskii equation [27, 36, 25]. If a harmonic trap potential is included, the equation becomes

$$i\hbar \frac{\partial \psi(\mathbf{x}, t)}{\partial t} = -\frac{\hbar^2}{2m} \nabla^2 \psi(\mathbf{x}, t) + \frac{m}{2} (\omega_x^2 x^2 + \omega_y^2 y^2 + \omega_z^2 z^2) \psi(\mathbf{x}, t) + NU_0 |\psi(\mathbf{x}, t)|^2 \psi(\mathbf{x}, t), \quad (2.1)$$

where $\mathbf{x} = (x, y, z)^T$ is the spatial coordinate vector, m is the atomic mass, $\hbar = 1.05 \times 10^{-34}$ [J s] is the Planck constant, N is the number of atoms in the condensation, and ω_x, ω_y and ω_z are the angular trap frequencies in x, y and z -direction, respectively. For the following we assume (w.r.o.g.) $\omega_x \leq \omega_y \leq \omega_z$. When $\omega_x = \omega_y = \omega_z$, the trap potential is isotropic. U_0 describes the interaction between atoms in the condensation and has the form

$$U_0 = \frac{4\pi\hbar^2 a}{m}, \quad (2.2)$$

where a is the s -wave scattering length (positive for repulsive interaction and negative for attractive interaction). It is necessary to ensure that the wave function is properly normalized. Specifically, we require

$$\int_{\mathbb{R}^3} |\psi(\mathbf{x}, t)|^2 d\mathbf{x} = 1. \quad (2.3)$$

A typical set of parameters used in current experiments with ^{87}Rb is

$$\begin{aligned} m &= 1.44 \times 10^{-25} \text{ [kg]}, \quad \omega_x = \omega_y = \omega_z = 20\pi \text{ [1/s]}, \\ a &= 5.1 \text{ [nm]} = 5.1 \times 10^{-9} \text{ [m]}, \quad N : 10^2 \sim 10^7. \end{aligned}$$

2.1 Dimensionless GPE

Following the physical literatures [21, 28, 38, 19, 24], in order to scale the equation (2.1) under the normalization (2.3), we introduce

$$\tilde{t} = \omega_x t, \quad \tilde{\mathbf{x}} = \frac{\mathbf{x}}{a_0}, \quad \tilde{\psi}(\tilde{\mathbf{x}}, \tilde{t}) = a_0^{3/2} \psi(\mathbf{x}, t), \quad \text{with} \quad a_0 = \sqrt{\frac{\hbar}{\omega_x m}}, \quad (2.4)$$

where a_0 is the length of the harmonic oscillator ground state. In fact, here we choose $1/\omega_x$ and a_0 as the dimensionless time and length units, respectively. Plugging (2.4) into (2.1), multiplying by $\frac{1}{m\omega_x^2 a_0^{1/2}}$, and then removing all \sim , we get the following dimensionless Gross-Pitaevskii equation under the normalization (2.3) in three dimension

$$i \frac{\partial \psi(\mathbf{x}, t)}{\partial t} = -\frac{1}{2} \nabla^2 \psi(\mathbf{x}, t) + V(\mathbf{x}) \psi(\mathbf{x}, t) + \kappa |\psi(\mathbf{x}, t)|^2 \psi(\mathbf{x}, t), \quad (2.5)$$

where

$$V(\mathbf{x}) = \frac{1}{2} (x^2 + \gamma_y^2 y^2 + \gamma_z^2 z^2), \quad \gamma_y = \frac{\omega_y}{\omega_x}, \quad \gamma_z = \frac{\omega_z}{\omega_x}, \quad \kappa = \frac{U_0 N}{a_0^3 \hbar \omega_x} = \frac{4\pi a N}{a_0}.$$

If we plug the typical set of parameters into above parameters, we find the values

$$a_0 \approx 0.3407 \times 10^{-5} \text{ [m]}, \quad \kappa \approx 0.01881 N : 1.881 \sim 188100.$$

There are two extreme regimes: one is when $\kappa = o(1)$, then equation (2.5) describes a weakly interacting condensation. The other one is when $\kappa \gg 1$, then (2.5) corresponds to a strongly interacting condensation or to the semiclassical regime.

2.2 Reduction to lower dimension

In the following two cases, the 3d Gross-Pitaevskii equation (2.5) can approximately be reduced to 2d or even 1d [29, 31]. In the case (disk-shaped condensation)

$$\omega_x \approx \omega_y, \quad \omega_z \gg \omega_x, \quad \Longleftrightarrow \quad \gamma_y \approx 1, \quad \gamma_z \gg 1, \quad (2.6)$$

the 3d GPE (2.5) can be reduced to 2d GPE with $\mathbf{x} = (x, y)^T$ by assuming that the time evolution does not cause excitations along the z -axis since they have a large energy of approximately $\hbar\omega_z$ compared to excitations along the x and y -axis with energies of about $\hbar\omega_x$. Thus we may assume that the condensation wave function along the z -axis is always well described by the ground state wave function and set [29, 31]

$$\psi = \psi_2(x, y, t)\psi_3(z) \quad \text{with} \quad \psi_3(z) = \left(\int_{\mathbb{R}^2} |\phi_g(x, y, z)|^2 dx dy \right)^{1/2}, \quad (2.7)$$

where $\phi_g(x, y, z)$ (see detail in (3.6)) is the ground state solution of the 3d GPE (2.5). Plugging (2.7) into (2.5), then multiplying by $\psi_3^*(z)$ (where f^* denotes the conjugate of a function f), integrating with respect to z over $(-\infty, \infty)$, we get

$$i \frac{\partial \psi_2(\mathbf{x}, t)}{\partial t} = -\frac{1}{2} \nabla^2 \psi_2 + \frac{1}{2} (x^2 + \gamma_y^2 y^2 + C) \psi_2 + \left(\kappa \int_{-\infty}^{\infty} \psi_3^4(z) dz \right) |\psi_2|^2 \psi_2, \quad (2.8)$$

where

$$C = \gamma_z^2 \int_{-\infty}^{\infty} z^2 |\psi_3(z)|^2 dz + \int_{-\infty}^{\infty} \left| \frac{d\psi_3}{dz} \right|^2 dz.$$

Since this GPE is time-transverse invariant, we can replace $\psi_2 \rightarrow \psi e^{-i\frac{Ct}{2}}$ which drops the constant C in the trap potential and obtain the 2d GPE, i.e.

$$i \frac{\partial \psi(\mathbf{x}, t)}{\partial t} = -\frac{1}{2} \nabla^2 \psi + \frac{1}{2} (x^2 + \gamma_y^2 y^2) \psi + \left(\kappa \int_{-\infty}^{\infty} \psi_3^4(z) dz \right) |\psi|^2 \psi. \quad (2.9)$$

The observables are not affected by this.

In the case (cigar-shaped condensation) [29, 31]

$$\omega_y \gg \omega_x, \quad \omega_z \gg \omega_x, \quad \Longleftrightarrow \quad \gamma_y \gg 1, \quad \gamma_z \gg 1, \quad (2.10)$$

the 3d GPE (2.5) can be reduced to 1d GPE with $\mathbf{x} = x$. Similarly to the 2d case, we derive the 1d GPE [29, 31]

$$i \frac{\partial \psi(x, t)}{\partial t} = -\frac{1}{2} \psi_{xx}(x, t) + \frac{x^2}{2} \psi(x, t) + \left(\kappa \int_{\mathbb{R}^2} \psi_{23}^4(y, z) dy dz \right) |\psi(x, t)|^2 \psi(x, t), \quad (2.11)$$

where

$$\psi_{23}(y, z) = \left(\int_{-\infty}^{\infty} |\phi_g(x, y, z)|^2 dx \right)^{1/2}, \quad (2.12)$$

with $\phi_g(x, y, z)$ (see (3.6)) the ground state solution of (2.5).

In fact, the 3d GPE (2.5), 2d GPE (2.9) and 1d GPE (2.11) can be written in a unified way [31]

$$i \frac{\partial \psi(\mathbf{x}, t)}{\partial t} = -\frac{1}{2} \nabla^2 \psi(\mathbf{x}, t) + V_d(\mathbf{x}) \psi(\mathbf{x}, t) + \kappa_d |\psi(\mathbf{x}, t)|^2 \psi(\mathbf{x}, t), \quad \mathbf{x} \in \mathbb{R}^d, \quad (2.13)$$

where

$$\kappa_d = \begin{cases} \kappa \int_{\mathbb{R}^2} \psi_{23}^4(y, z) dy dz, \\ \kappa \int_{-\infty}^{\infty} \psi_3^4(z) dz, \\ \kappa, \end{cases} \quad V_d(\mathbf{x}) = \begin{cases} \frac{1}{2} x^2, & d = 1, \\ \frac{1}{2} (x^2 + \gamma_y^2 y^2), & d = 2, \\ \frac{1}{2} (x^2 + \gamma_y^2 y^2 + \gamma_z^2 z^2), & d = 3. \end{cases} \quad (2.14)$$

The normalization condition to (2.13) is

$$\int_{\mathbb{R}^d} |\psi(\mathbf{x}, t)|^2 d\mathbf{x} = 1. \quad (2.15)$$

3 Ground state solution

In this section, we will propose a new numerical method by directly minimizing the energy functional via finite element discretization to compute the ground state solution of a BEC (2.13). Furthermore we will also provide approximate ground state solutions in two extreme regimes: very weak interactions and strong repulsive interactions.

3.1 Minimization problem

To find a stationary solution of (2.13), we write

$$\psi(\mathbf{x}, t) = e^{-i\mu t} \phi(\mathbf{x}), \quad (3.1)$$

where μ is the chemical potential of the condensation and ϕ a real-valued function independent of time. Inserting into (2.13) gives the following equation for $\phi(\mathbf{x})$

$$\mu \phi(\mathbf{x}) = -\frac{1}{2} \nabla^2 \phi(\mathbf{x}) + V_d(\mathbf{x}) \phi(\mathbf{x}) + \kappa_d |\phi(\mathbf{x})|^2 \phi(\mathbf{x}), \quad \mathbf{x} \in \mathbb{R}^d, \quad (3.2)$$

under the normalization condition

$$\int_{\mathbb{R}^d} |\phi(\mathbf{x})|^2 d\mathbf{x} = 1. \quad (3.3)$$

This is a nonlinear eigenvalue problem under a constraint and any eigenvalue μ can be computed from its corresponding eigenfunction ϕ by

$$\mu = \mu_\kappa(\phi) = \int_{\mathbb{R}^d} \left[\frac{1}{2} |\nabla \phi(\mathbf{x})|^2 + V_d(\mathbf{x}) \phi^2(\mathbf{x}) + \kappa_d \phi^4(\mathbf{x}) \right] d\mathbf{x}. \quad (3.4)$$

The Bose-Einstein condensation ground-state wave function $\phi_g(\mathbf{x})$ is found by solving this eigenvalue problem under the normalization condition (3.3) with the minimized chemical potential μ_g . Usually, the ground state problem is formulated variationally. Define the energy functional

$$E_\kappa(\phi) := \int_{\mathbb{R}^3} \left[\frac{1}{2} |\nabla \phi|^2 + V_d(x) |\phi|^2 + \frac{\kappa}{2} |\phi|^4 \right] d\mathbf{x}. \quad (3.5)$$

It is easy to see that critical points of the energy functional $E_\kappa(\phi)$ under the constraint (3.3) are eigenfunctions of the nonlinear eigenvalue problem (3.2) under the constraint (3.3) and versus versa. In fact, (3.2) can be viewed as the Euler-Lagrange equation of the energy functional $E_\kappa(\phi)$ under the constraint (3.3). To compute the ground state ϕ_g , we solve the minimization problem

(V) Find $(\mu_g, \phi_g \in V)$ such that

$$E_\kappa(\phi_g) = \min_{\phi \in V} E_\kappa(\phi), \quad \mu_g = \mu_\kappa(\phi_g) = E_\kappa(\phi_g) + \int_{\mathbb{R}^d} \frac{\kappa_d}{2} \phi_g^4(\mathbf{x}) d\mathbf{x}, \quad (3.6)$$

where the set V is defined as

$$V = \left\{ \phi \mid E_\kappa(\phi) < \infty, \int_{\mathbb{R}^d} |\phi(\mathbf{x})|^2 d\mathbf{x} = 1 \right\}.$$

In non-rotating BEC, the minimization problem (3.6) has a unique real valued nonnegative ground state solution $\phi_g(\mathbf{x}) > 0$ for $\mathbf{x} \in \mathbb{R}^d$ [32]. In physical literatures, the minimizer of (3.6) was obtained by either the Runge-Kutta type method [21, 2, 3] or the imaginary time method [6, 16, 14]. Here we present a method by directly minimizing the energy functional $E_\kappa(\phi)$ through the finite element discretization [17].

3.2 Approximation in a bounded domain

The eigenvalue problem (3.2) and the minimization problem (3.6) are defined in \mathbb{R}^d . In practical computation, usually they are approximated by problems defined on a bounded computational domain. Since the full wave function must vanish exponentially fast as $|\mathbf{x}| \rightarrow \infty$ and due to symmetry, choosing $R_1, \dots, R_d > 0$ sufficiently large and denoting

$$\Omega^R = [0, R_1] \times \dots \times [0, R_d],$$

then the minimization problem (3.6) can be approximated by

(V^R) Find $(\mu_g^R, \phi_g^R \in V_g)$ such that

$$E_\kappa^R(\phi_g^R) = \min_{\phi \in V_g} E_\kappa^R(\phi), \quad \mu_g^R = E_\kappa^R(\phi_g^R) + \int_{\Omega^R} \frac{\kappa_d}{2} [\phi_g^R(\mathbf{x})]^4 d\mathbf{x}, \quad (3.7)$$

where the set V_g and the functional $E_\kappa^R(\phi)$ are defined as

$$V_g = \left\{ \phi \mid E_\kappa^R(\phi) < \infty, \ 2^d \int_{\Omega^R} |\phi(\mathbf{x})|^2 d\mathbf{x} = 1, \ \phi(R_1, x_2, \dots, x_d) = \dots = \phi(x_1, \dots, x_{d-1}, R_d) = 0 \right\},$$

$$E_\kappa^R(\phi) = 2^d \int_{\Omega^R} \left[\frac{1}{2} |\nabla \phi(\mathbf{x})|^2 + V_d(\mathbf{x}) |\phi(\mathbf{x})|^2 + \frac{\kappa_d}{2} |\phi(\mathbf{x})|^4 \right] d\mathbf{x}.$$

3.3 Discretization

The functional $E_\kappa^R(\phi)$ in (3.7) (or $E_\kappa(\phi)$ in (3.6)) can be discretized by the finite element method [17], finite difference method [34] or spectral method [26]. Here we use the finite element method because it can easily keep the good properties of $E_\kappa^R(\phi)$, e.g. positive, coercive and weakly lower semicontinuous when $\kappa_d \geq 0$, on the unit sphere in finite dimensions. Let

$$\tilde{V}_g = \left\{ \phi \mid E_\kappa^R(\phi) < \infty, \ \phi(R_1, x_2, \dots, x_d) = \dots = \phi(x_1, \dots, x_{d-1}, R_d) = 0 \right\}$$

and \tilde{V}_g^h be a finite dimensional subspace of \tilde{V}_g [17], i.e. $\tilde{V}_g^h \subset \tilde{V}_g$. Then the finite dimensional set

$$V_g^h = \left\{ \phi^h \in \tilde{V}_g^h \mid 2^d \int_{\Omega^R} |\phi^h(\mathbf{x})|^2 d\mathbf{x} = 1, \right\}$$

is a subset of V_g , i.e. $V_g^h \subset V_g$. Thus the minimization problem (3.7) can be approximated by

(V^{R,h}) Find $(\mu_g^{R,h}, \phi_g^{R,h} \in V_g^h)$ such that

$$E_\kappa^R(\phi_g^{R,h}) = \min_{\phi^h \in V_g^h} E_\kappa^R(\phi^h), \quad \mu_g^{R,h} = E_\kappa^R(\phi_g^{R,h}) + \int_{\Omega^R} \frac{\kappa_d}{2} [\phi_g^{R,h}(\mathbf{x})]^4 d\mathbf{x}. \quad (3.8)$$

Introducing a functional with a Lagrange multiplier corresponding to the normalization condition (3.3), i.e.

$$\begin{aligned} \tilde{E}_\kappa^R(\phi^h, \lambda) &= E_\kappa^R(\phi^h) - \lambda \left(2^d \int_{\Omega^R} |\phi^h(\mathbf{x})|^2 d\mathbf{x} - 1 \right) \\ &\equiv F(\Phi^h, \lambda), \quad \phi^h \in \tilde{V}_g^h, \quad \lambda \in \mathbb{R}, \end{aligned}$$

where $\phi^h(\mathbf{x}) = \Psi^h(\mathbf{x}) \cdot \Phi^h \equiv \sum_{j=1}^M \Psi_1^h(\mathbf{x}) \Phi_j^h$ with $\Psi^h(\mathbf{x}) = (\Psi_1^h(\mathbf{x}), \dots, \Psi_M^h(\mathbf{x}))^T$ a basis of the finite element subspace \tilde{V}_g^h and $\Phi^h = (\Phi_1^h, \dots, \Phi_M^h)^T$ the unknowns of

$\phi^h(\mathbf{x})$ [17], then the minimizer $\phi_g^{R,h} = \Psi^h(\mathbf{x}) \cdot \Phi_g^{R,h}$ of the minimization problem (3.8) is a critical point of the functional $\tilde{E}_\kappa^R(\phi^h, \lambda)$. This implies

$$\nabla_{\Phi^h} F(\Phi^h, \lambda) \Big|_{\Phi^h = \Phi_g^{R,h}} = \mathbf{0}, \quad \frac{\partial F(\Phi^h, \lambda)}{\partial \lambda} \Big|_{\Phi^h = \Phi_g^{R,h}} = 0. \quad (3.9)$$

The nonlinear system (3.9) is solved by the Newton's method [35] or quasi-Newton's method [35] with a proper choice of the initial data $(\phi_g^{R,h})^{(0)} = \Psi^h(\mathbf{x}) \cdot (\Phi_g^{R,h})^{(0)}$ and $\lambda^{(0)}$ is the least square solution of

$$\nabla_{\Phi^h} F(\Phi^h, \lambda) \Big|_{(\Phi^h = (\Phi_g^{R,h})^{(0)}, \lambda = \lambda^{(0)})} = \mathbf{0}.$$

The initial guess $(\phi_g^{R,h})^{(0)}$ is chosen as the interpolant on \tilde{V}_g^h of the approximate ground state solution for very weak interactions (4.13) or strong repulsive interactions (4.15) when κ_d is not too big or not too small, respectively. These approximate ground state solutions are given in the next subsection. Another way to choose the initial guess is to use a continuation technique, i.e. use the numerical solution of the ground state function for a small κ_d as initial guess for computing the solution of a larger κ_d .

3.4 Approximate ground state solution

Here we present the approximate ground state solution of (3.2) in two extreme regimes: very weak interactions and strong repulsive interactions. These approximate ground state solutions are used as initial guess $(\phi_g^{R,h})^{(0)}$ in our practical computation of the minimization problem (3.8) (or (3.9)).

For a very weakly interacting condensation, i.e. $\kappa_d = o(1)$, we drop the nonlinear term (i.e. the last term on the right hand side of (3.2)) and get [31]

$$\mu \phi(\mathbf{x}) = -\frac{1}{2} \nabla^2 \phi(\mathbf{x}) + V_d(\mathbf{x}) \phi(\mathbf{x}), \quad \mathbf{x} \in \mathbb{R}^d. \quad (3.10)$$

The ground state solution of (3.10) is

$$\mu_d^w = \frac{1}{2} \begin{cases} 1, \\ 1 + \gamma_y, \\ 1 + \gamma_y + \gamma_z, \end{cases} \quad \phi_d^w(\mathbf{x}) = \frac{1}{(\pi)^{d/4}} \begin{cases} e^{-x^2/2}, & d = 1, \\ \gamma_y^{1/4} e^{-(x^2 + \gamma_y y^2)/2}, & d = 2, \\ (\gamma_y \gamma_z)^{1/4} e^{-(x^2 + \gamma_y y^2 + \gamma_z z^2)/2}, & d = 3. \end{cases} \quad (3.11)$$

This can be viewed as an approximate ground state solution of (2.13) in the case of a very weakly interacting condensation.

For strong repulsive interactions, i.e. $\kappa_d \gg 1$, we drop the diffusion term (i.e. the first term on the right hand side of (3.2)) corresponding to the Thomas-Fermi approximation [31]:

$$\mu \phi(\mathbf{x}) = V_d(\mathbf{x}) \phi(\mathbf{x}) + \kappa_d |\phi(\mathbf{x})|^2 \phi(\mathbf{x}), \quad \mathbf{x} \in \mathbb{R}^d, \quad (3.12)$$

The ground state solution of (3.12) is the compactly supported function $\phi_d^s(\mathbf{x})$:

$$\mu_d^s = \begin{cases} \frac{1}{2} \left(\frac{3\kappa_1}{2} \right)^{2/3}, & d = 1, \\ \left(\frac{\kappa_2 \gamma_y}{\pi} \right)^{1/2}, & d = 2, \\ \frac{1}{2} \left(\frac{15\kappa_3 \gamma_y \gamma_z}{4\pi} \right)^{2/5}, & d = 3; \end{cases} \quad (3.13)$$

$$\phi_d^s(\mathbf{x}) = \begin{cases} \sqrt{(\mu_d^s - V_d(\mathbf{x}))/\kappa_d}, & V_d(\mathbf{x}) < \mu_d^s, \\ 0, & \text{otherwise.} \end{cases} \quad (3.14)$$

Remark 3.1 *As indicated in Figure 6, an interface layer correction has to be constructed in order to improve the approximation quality in the Thomas-Fermi regime (i.e. $\kappa_d \gg 1$). For a convergence proof of $\phi_3^s \rightarrow \phi_g$ as $\kappa_3 \rightarrow +\infty$ (without convergence rate) we refer to [32]. In Section 6, these convergence rates are reported based on our numerical solutions.*

4 Ground state solution in 1d, 2d with radial symmetry and 3d with spherical symmetry

In this section, we present detailed numerical formula and its finite element approximation for the ground state solution of GPE in 1d, 2d with radial symmetry (i.e. $\gamma_y = 1$) and 3d with spherical symmetry (i.e. $\gamma_y = \gamma_z = 1$). In these cases, the problem is reduced to 1d. Due to symmetry, the GPE (2.13) essentially collapses to a 1d problem with $r = |\mathbf{x}| \in [0, \infty)$ for $d = 1, 2, 3$

$$i \frac{\partial \psi(r, t)}{\partial t} = -\frac{1}{2} \frac{1}{r^{d-1}} \frac{\partial}{\partial r} \left(r^{d-1} \frac{\partial}{\partial r} \psi(r, t) \right) + \frac{r^2}{2} \psi(r, t) + \kappa_d |\psi(r, t)|^2 \psi(r, t), \quad (4.1)$$

$$\frac{\partial \psi(0, t)}{\partial r} = 0, \quad \psi(r, t) \rightarrow 0, \quad \text{when } r \rightarrow \infty. \quad (4.2)$$

The normalization condition collapses to

$$C_d \int_0^\infty |\psi(r, t)|^2 r^{d-1} dr = 1, \quad (4.3)$$

where

$$C_d = \begin{cases} 2, & d = 1, \\ 2\pi, & d = 2, \\ 4\pi, & d = 3. \end{cases}$$

4.1 Minimization problem

The eigenvalue problem (3.2) collapses to

$$\mu \phi(r) = -\frac{1}{2} \frac{1}{r^{d-1}} \frac{d}{dr} \left(r^{d-1} \frac{d}{dr} \phi(r) \right) + \frac{r^2}{2} \phi(r) + \kappa_d |\phi(r)|^2 \phi(r), \quad 0 < r < \infty, \quad (4.4)$$

$$\phi'(0) = 0, \quad \phi(r) \rightarrow 0, \quad \text{when } r \rightarrow \infty, \quad (4.5)$$

under the normalization condition

$$C_d \int_0^\infty |\phi(r)|^2 r^{d-1} dr = 1. \quad (4.6)$$

The minimization problem (3.6) collapses to

(V) Find $(\mu_g, \phi_g \in V)$ such that

$$E_\kappa(\phi_g) = \min_{\phi \in V} E_\kappa(\phi), \quad \mu_g = E_\kappa(\phi_g) + C_d \int_0^\infty \frac{\kappa_d}{2} \phi_g^4(r) r^{d-1} dr, \quad (4.7)$$

where the set V and the energy functional $E_\kappa(\phi)$ are defined as

$$V = \left\{ \phi \mid E_\kappa(\phi) < \infty, C_d \int_0^\infty |\phi(r)|^2 r^{d-1} dr = 1 \right\},$$

$$E_\kappa(\phi) = C_d \int_0^\infty \frac{r^{d-1}}{2} \left[[\phi'(r)]^2 + r^2 \phi^2(r) + \kappa_d \phi^4(r) \right] dr.$$

4.2 Approximation in a bounded domain

The eigenvalue problem (4.4), (4.5) and the minimization problem (4.7) are defined in a semi-infinite interval $(0, \infty)$. In practical computation, usually they are approximated by problems defined on a finite interval. Since the full wave function must vanish exponentially fast as $r \rightarrow \infty$, choosing $R > 0$ sufficiently large, then the eigenvalue problem (4.4), (4.5) can be approximated by

$$\mu \phi(r) = -\frac{1}{2} \frac{1}{r^{d-1}} \frac{d}{dr} \left(r^{d-1} \frac{d}{dr} \phi(r) \right) + \frac{r^2}{2} \phi(r) + \kappa_d |\phi(r)|^2 \phi(r), \quad 0 < r < R, \quad (4.8)$$

$$\phi'(0) = 0, \quad \phi(R) = 0, \quad (4.9)$$

under the normalization condition

$$C_d \int_0^R |\phi(r)|^2 r^{d-1} dr = 1. \quad (4.10)$$

Similarly the minimization problem (4.7) can be approximated by

(V^R) Find $(\mu_g^R, \phi_g^R \in V_g)$ such that

$$E_\kappa^R(\phi_g^R) = \min_{\phi \in V_g} E_\kappa^R(\phi), \quad \mu_g^R = E_\kappa^R(\phi_g^R) + C_d \int_0^R \frac{\kappa_d}{2} [\phi_g^R(r)]^4 r^{d-1} dr, \quad (4.11)$$

where the set V_g and the functional $E_\kappa^R(\phi)$ are defined as

$$V_g = \left\{ \phi \mid E_\kappa^R(\phi) < \infty, C_d \int_0^R |\phi(r)|^2 r^{d-1} dr = 1, \phi(R) = 0 \right\},$$

$$E_\kappa^R(\phi) = C_d \int_0^R \frac{r^{d-1}}{2} \left[[\phi'(r)]^2 + r^2 \phi^2(r) + \kappa_d \phi^4(r) \right] dr.$$

4.3 Finite element approximation

Assume that

$$0 = r_0 < r_1 < r_2 < \cdots < r_M = R$$

is a partition of the interval $[0, R]$ with mesh size h [17]. Let

$$\begin{aligned} \tilde{V}_g^h &= \left\{ \phi^h(r) \in C([0, R]) \mid \phi^h(r)|_{[r_j, r_{j+1}]} \in P_1([r_j, r_{j+1}]), \quad 0 \leq j \leq M-1, \right. \\ &\quad \left. \phi^h(R) = 0 \right\}, \\ V_g^h &= \left\{ \phi^h \in \tilde{V}_g^h \mid C_d \int_0^R |\phi^h(r)|^2 r^{d-1} dr = 1, \right\}; \end{aligned}$$

where P_1 denotes piecewise linear polynomials. Then the finite element approximation of the problem (4.7) is

$(V^{R,h})$ Find $(\mu_g^{R,h}, \phi_g^{R,h} \in V_g^h)$ such that

$$E_\kappa^R(\phi_g^{R,h}) = \min_{\phi \in V_g^h} E_\kappa^R(\phi), \quad \mu_g^{R,h} = E_\kappa^R(\phi_g^{R,h}) + C_d \int_0^R \frac{\kappa_d}{2} [\phi_g^{R,h}(r)]^4 r^{d-1} dr. \quad (4.12)$$

4.4 Approximate ground state solution

In these cases, the approximate ground state solution collapses to the following. For a very weakly interacting condensation, i.e. $\kappa_d = o(1)$, the ground state solution is

$$\mu_d^w = \frac{d}{2}, \quad \phi_d^w(r) = \frac{1}{\pi^{d/4}} e^{-r^2/2}, \quad d = 1, 2, 3. \quad (4.13)$$

For strong repulsive interactions, i.e. $\kappa_d \gg 1$, the ground state solution is

$$\mu_d^s = \frac{1}{2} \left[\frac{((d+1)^2 - 1)\kappa_d}{C_d} \right]^{2/(d+2)}, \quad d = 1, 2, 3, \quad (4.14)$$

$$\phi_d^s(r) = \begin{cases} \sqrt{(\mu_d^s - r^2/2)/\kappa_d}, & r^2 < 2\mu_d^s, \\ 0, & \text{otherwise,} \end{cases} \quad d = 1, 2, 3. \quad (4.15)$$

5 Ground state solution in 3d with cylindrical symmetry

In this section, we present detailed numerical formula and its finite element approximation for the ground state solution of GPE in 3d with cylindrical symmetry (i.e. $\gamma_y = 1$). In this case, the problem is reduced to 2d. Due to symmetry, the GPE (2.13) essentially collapses to a 2d problem with $r = \sqrt{x^2 + y^2} \in [0, \infty)$

$$i \frac{\partial \psi(r, z, t)}{\partial t} = -\frac{1}{2} \left[\frac{1}{r} \frac{\partial}{\partial r} \left(r \frac{\partial \psi}{\partial r} \right) + \frac{\partial^2 \psi}{\partial z^2} \right] + \frac{1}{2} (r^2 + \gamma_z^2 z^2) \psi + \kappa |\psi|^2 \psi, \quad (5.1)$$

$$\begin{aligned} 0 < r, z < \infty, \\ \frac{\partial \psi(0, z, t)}{\partial r} = 0, \quad 0 \leq z < \infty, \quad \frac{\partial \psi(r, 0, t)}{\partial z} = 0, \quad 0 \leq r < \infty, \end{aligned} \quad (5.2)$$

$$\psi(r, z, t) \rightarrow 0, \quad \text{when } r + |z| \rightarrow \infty. \quad (5.3)$$

The normalization condition collapses to

$$4\pi \int_0^\infty \int_0^\infty |\psi(r, z, t)|^2 r \, dr dz = 1. \quad (5.4)$$

5.1 Minimization problem

The eigenvalue problem (3.2) collapses to

$$\mu \phi(r, z) = -\frac{1}{2} \left[\frac{1}{r} \frac{\partial}{\partial r} \left(r \frac{\partial \phi}{\partial r} \right) + \frac{\partial^2 \phi}{\partial z^2} \right] + \frac{1}{2} (r^2 + \gamma_z^2 z^2) \phi + \kappa |\phi|^2 \phi, \quad (5.5)$$

$$\begin{aligned} 0 < r, z < \infty, \\ \frac{\partial \phi(0, z)}{\partial r} = 0, \quad 0 \leq z < \infty, \quad \frac{\partial \phi(r, 0)}{\partial z} = 0, \quad 0 \leq r < \infty, \end{aligned} \quad (5.6)$$

$$\phi(r, z) \rightarrow 0, \quad \text{when } r + |z| \rightarrow \infty, \quad (5.7)$$

under the normalization condition

$$4\pi \int_0^\infty \int_0^\infty |\phi(r, z)|^2 r \, dr dz = 1. \quad (5.8)$$

The minimization problem (3.6) collapses to

(V) Find $(\mu_g, \phi_g \in V)$ such that

$$E_\kappa(\phi_g) = \min_{\phi \in V} E_\kappa(\phi), \quad \mu_g = E_\kappa(\phi_g) + 4\pi \int_0^\infty \int_0^\infty \frac{\kappa}{2} \phi_g^4(r, z) r \, dr dz, \quad (5.9)$$

where the set V and the functional $E_\kappa(\phi)$ are defined as

$$\begin{aligned} V &= \left\{ \phi \mid E_\kappa(\phi) < \infty, \, 4\pi \int_0^\infty \int_0^\infty |\phi(r, z)|^2 r \, dr dz = 1 \right\}, \\ E_\kappa(\phi) &= 4\pi \int_0^\infty \int_0^\infty \frac{r}{2} \left[\phi_r^2(r, z) + \phi_z^2(r, z) + (r^2 + \gamma_z^2 z^2) \phi^2(r, z) + \kappa \phi^4(r, z) \right] dr dz. \end{aligned}$$

5.2 Approximation in a bounded domain

The eigenvalue problem (5.5)-(5.7) and the minimization problem (5.9) are defined in the first quadrant of the rz -plane. In practical computation, usually they are approximated by problems defined on a bounded domain. Since the full wave function must vanish exponentially fast as $r + |z| \rightarrow \infty$, choosing $R > 0$ and $Z > 0$

sufficiently large, then the eigenvalue problem (5.5)-(5.7) can be approximated by

$$\mu \phi(r, z) = -\frac{1}{2} \left[\frac{1}{r} \frac{\partial}{\partial r} \left(r \frac{\partial \phi}{\partial r} \right) + \frac{\partial^2 \phi}{\partial z^2} \right] + \frac{1}{2} (r^2 + \gamma_z^2 z^2) \phi + \kappa |\phi|^2 \phi, \quad 0 < r < R, \quad 0 < z < Z, \quad (5.10)$$

$$\frac{\partial \phi(0, z)}{\partial r} = 0, \quad 0 \leq z \leq Z, \quad \frac{\partial \phi(r, 0)}{\partial z} = 0, \quad 0 \leq r \leq R, \quad (5.11)$$

$$\phi(R, z) = 0, \quad 0 \leq z \leq Z, \quad \phi(r, Z) = 0, \quad 0 \leq r \leq R, \quad (5.12)$$

under the normalization condition

$$4\pi \int_0^R \int_0^Z |\phi(r, z)|^2 r \, dz dr = 1. \quad (5.13)$$

Similarly the minimization problem (5.9) can be approximated by

(V^R) Find $(\mu_g^R, \phi_g^R \in V_g)$ such that

$$E_\kappa^R(\phi_g^R) = \min_{\phi \in V_g} E_\kappa^R(\phi), \quad \mu_g^R = E_\kappa^R(\phi_g^R) + 4\pi \int_0^R \int_0^Z \frac{\kappa}{2} [\phi_g^R(r, z)]^4 r \, dr dz, \quad (5.14)$$

where the set V_g and the functional $J^R(\phi)$ are defined as

$$V_g = \left\{ \phi \mid E_\kappa^R(\phi) < \infty, \quad 4\pi \int_0^R \int_0^Z |\phi(r, z)|^2 r \, dz dr = 1, \right. \\ \left. \phi(R, z) = 0, \quad 0 \leq z \leq Z, \quad \phi(r, Z) = 0, \quad 0 \leq r \leq R \right\}, \\ E_\kappa^R(\phi) = 4\pi \int_0^R \int_0^Z \frac{r}{2} [\phi_r^2(r, z) + \phi_z^2(r, z) + (r^2 + \gamma_z^2 z^2) \phi^2(r, z) + \kappa \phi^4(r, z)] \, dz dr.$$

5.3 Finite element approximation

Assume that

$$0 = r_0 < r_1 < r_2 < \cdots < r_M = R, \quad 0 = z_0 < z_1 < z_2 < \cdots < z_N = Z$$

is a partition of the rectangle $[0, R] \times [0, Z]$ with mesh size h [17]. Let

$$\tilde{V}_g^h = \left\{ \phi^h(r, z) \in C([0, R] \times [0, Z]) \mid \phi^h(r, z)|_{[r_j, r_{j+1}] \times [z_l, z_{l+1}]} \in Q_1([r_j, r_{j+1}] \times [z_l, z_{l+1}]), \right. \\ \left. 0 \leq j \leq M-1, \quad 0 \leq l \leq N-1, \quad \phi^h(R, z) = 0, \quad 0 \leq z \leq Z, \right. \\ \left. \phi^h(r, Z) = 0, \quad 0 \leq r \leq R \right\}, \\ V_g^h = \left\{ \phi^h \in \tilde{V}_g^h \mid 4\pi \int_0^R \int_0^Z |\phi^h(r, z)|^2 r \, dz dr = 1 \right\};$$

where Q_1 denotes all bilinear polynomials. Then the finite element approximation of the problem (5.14) is

($V^{R,h}$) Find $(\mu_g^{R,h}, \phi_g^{R,h} \in V_g^h)$ such that

$$E_\kappa^R(\phi_g^{R,h}) = \min_{\phi \in V_g^h} E_\kappa^R(\phi), \quad \mu_g^{R,h} = E_\kappa^R(\phi_g^{R,h}) + 4\pi \int_0^R \int_0^Z \frac{\kappa}{2} [\phi_g^{R,h}(r, z)]^4 r \, dr dz. \quad (5.15)$$

5.4 Approximate ground state solution

In this case, the approximate ground state solution collapses to the following. For a very weakly interacting condensation, i.e. $\kappa_3 = \kappa = o(1)$, the ground state solution is

$$\mu_3^w = 1 + \frac{\gamma_z}{2}, \quad \phi_3^w(r, z) = \frac{\gamma_z^{1/4}}{(\pi)^{3/4}} e^{-(r^2 + \gamma_z z^2)/2}. \quad (5.16)$$

For strong repulsive interactions, i.e. $\kappa_3 = \kappa \gg 1$, the ground state solution is

$$\mu_3^s = \frac{1}{2} \left(\frac{15\kappa\gamma_z}{4\pi} \right)^{2/5}, \quad (5.17)$$

$$\phi_3^s(r, z) = \begin{cases} \sqrt{(\mu_3^s - (r^2 + \gamma_z^2 z^2)/2)/\kappa}, & r^2 + \gamma_z^2 z^2 < 2\mu_3^s, \\ 0, & \text{otherwise.} \end{cases} \quad (5.18)$$

6 Numerical results

In this section we shall report on numerical error analysis of our method, numerical ground state solutions of (2.13) in 1d, 2d with radial symmetry and 3d with spherical symmetry as well as cylindrical symmetry. Furthermore we also compare the numerical ground state solution of (2.13) in 3d and the corresponding Thomas-Fermi approximation (5.18). Convergence rates of the Thomas-Fermi approximations to their exact counterparts are also reported.

6.1 Numerical error analysis

In this subsection, we study numerically the convergence rate of the finite element discretization to the minimization problem (3.7) in 1d. We choose $d = 1$ and $\kappa_d = \kappa_1 = 62.742$ in (4.11). We compute a numerical solution of (4.11) in 1d on $\Omega = [0, 8]$ by using the discretization (4.12) with a very fine mesh, e.g. $h = \frac{1}{128}$, as the “exact” ground state solution $\phi_g(x)$. Table 1 shows the errors $E_\kappa(\phi_g^h) - E_\kappa(\phi_g)$, $\mu_g^h - \mu_g$, $\max |\phi_g^h(x) - \phi_g(x)|$, $\|\phi_g^h - \phi_g\|_{L^2(\Omega)}$, $\|(\phi_g^h)^2 - (\phi_g)^2\|_{L^1(\Omega)}$ and $\|\phi_g^h - \phi_g\|_{H^1(\Omega)}$ for different mesh size h . Here we use the standard Sobolev space norms [1].

From Table 1, we observe that the approximate energy $E_\kappa(\phi_g^h)$, chemical potential μ_g^h , ground state solution ϕ_g^h , and atom density function $(\phi_g^h)^2$ converge to $E_\kappa(\phi_g)$,

	$h = \frac{1}{2}$	$h = \frac{1}{4}$	$h = \frac{1}{8}$	$h = \frac{1}{16}$	$h = \frac{1}{32}$
$E_\kappa(\phi_g^h) - E_\kappa(\phi_g)$	6.528E-4	1.570E-4	3.878E-5	9.560E-6	2.274E-6
$\mu_g^h - \mu_g$	3.462E-4	8.073E-5	1.986E-5	4.887E-6	1.160E-6
$\max \phi_g^h(x) - \phi_g(x) $	3.222E-3	8.450E-4	2.091E-4	5.300E-5	1.359E-5
$\ \phi_g^h - \phi_g\ _{L^2(\Omega)}$	2.177E-3	5.290E-4	1.323E-4	3.394E-5	9.295E-6
$\ (\phi_g^h)^2 - (\phi_g)^2\ _{L^1(\Omega)}$	1.042E-3	2.633E-4	6.579E-5	1.700E-5	4.927E-6
$\ \phi_g^h - \phi_g\ _{H^1(\Omega)}$	2.493E-2	1.246E-2	6.218E-3	3.091E-3	1.508E-3

Table 1. Numerical error analysis of the finite element discretization (4.12).

μ_g , ϕ_g in maximum norm and L^2 -norm, and $(\phi_g)^2$ in L^1 -norm, respectively, at second order convergence rate when the mesh size h goes to zero. Furthermore ϕ_g^h converges to ϕ_g in H^1 -norm at first order convergence rate.

6.2 Results in 1d, 2d with radial symmetry and 3d with spherical symmetry

An interesting property of the condensation wave function in these cases is its root mean square (rms) size r_{rms} defined by

$$r_{\text{rms}}^2 = \langle r^2 \rangle = C_d \int_0^\infty r^2 \phi^2(r) r^{d-1} dr, \quad d = 1, 2, 3. \quad (6.1)$$

In our computations, we choose $R = 16$ in (4.8) with a uniform partition of the interval $[0, R]$ of mesh size $h = \frac{1}{50}$ in (4.12).

Figure 1 shows the ground-state condensation wave function $\phi_g(r)$ (with $\phi_g(-r) = \phi_g(r)$ for $r \in \mathbb{R}$ in 1d) versus r and the chemical potential μ_g for different κ_d , and Table 2 lists $\phi_g(0)$, r_{rms} , μ_g versus κ_d for $d = 1$. For comparison, we also list the chemical potential μ_g obtained by the Thomas-Fermi approximation (TFA) in (4.14). Furthermore Figure 2 and Table 3 show similar results for $d = 2$, and Figures 3 and Table 4 for $d = 3$.

From Figures 1-3 and Tables 2-4, we can see that the chemical potential μ_g and the root mean square size will increase when the interaction coefficient κ_d (i.e. the number of atoms in the condensation) is increasing. On the other hand, the peak of the ground state solution $\phi_g(0)$ will decrease. If we use the typical set of parameter values in Section 2, a $\kappa_3 = 31371$ corresponds to a condensation population of $N \approx 1\,667\,800$, i.e. approximately one and a half millions atoms in the condensation. Furthermore the Thomas-Fermi approximation gives accurate chemical potential μ_g

κ_1	$\phi_g(0)$	r_{rms}	μ_g	
			Numerical	TFA
-12.5484	1.7718	0.1444	-19.669	NA
-6.2742	1.2654	0.2810	-4.9553	NA
-2.5097	0.9132	0.5133	-0.8061	NA
0	0.7511	0.7071	0.5000	NA
3.1371	0.6459	0.8960	1.5265	NA
12.5484	0.5297	1.2454	3.5965	3.538
31.371	0.4556	1.6416	6.5526	6.517
62.742	0.4060	2.0495	10.369	10.345
156.855	0.3485	2.7679	19.0704	19.056
313.71	0.3105	3.4823	30.259	30.249
627.42	0.2766	4.3847	48.024	48.018
1254.8	0.2464	5.5228	76.226	76.222

Table 2. Ground state chemical potential μ_g , maximum value of the wave function $\phi_g(0)$ and root mean square size r_{rms} versus the interaction coefficient κ_d in 1d ($d = 1$).

κ_2	$\phi_g(0)$	r_{rms}	μ_g	
			Numerical	TFA
-5.8	2.1770	0.3208	-5.552	NA
-4.5	0.8948	0.7091	-0.2923	NA
-2.5097	0.6754	0.8775	0.4997	NA
0	0.5642	1.0000	1.0000	NA
3.1371	0.4913	1.1051	1.4200	NA
12.5484	0.3919	1.3068	2.2558	1.9986
62.742	0.2676	1.7881	4.6098	4.4689
313.71	0.1787	2.6044	10.068	9.9928
627.42	0.1502	3.0845	14.1892	14.132
1254.8	0.1262	3.6598	20.0286	19.9854

Table 3. Ground state chemical potential μ_g , maximum value of the wave function $\phi_g(0)$ and root mean square size r_{rms} versus the interaction coefficient κ_d in 2d with radial symmetry ($d = 2$).

κ_3	$\phi_g(0)$	r_{rms}	μ_g	
			Numerical	TFA
-7	0.7613	0.9512	0.6210	NA
-3.1371	0.4881	1.1521	1.2652	NA
0	0.4238	1.2248	1.5000	NA
3.1371	0.3843	1.2785	1.6774	NA
12.5484	0.3180	1.3921	2.0650	1.4762
31.371	0.2581	1.5356	2.5861	2.1298
125.484	0.1738	1.8821	4.0141	3.7082
627.4	0.1066	2.5057	7.2484	7.059
3137.1	0.0655	3.4145	13.553	13.438
31371	0.0328	5.3852	33.810	33.755

Table 4. Ground state chemical potential μ_g , maximum value of the wave function $\phi_g(0)$ and root mean square size r_{rms} versus the interaction coefficient κ_d in 3d with spherical symmetry ($d = 3$).

only when the interaction κ_d is very big and poor approximation for intermediate values of κ_d (cf. Tables 2-4).

Here we also report the convergence rates of the Thomas-Fermi approximations ϕ_d^s and μ_d^s to the exact ground state solution ϕ_g and μ_g , respectively, as $\frac{1}{\kappa_d} \rightarrow 0$. Tables 5,6&7 list these results for $d = 1, 2$ &3, respectively.

From Tables 5-7, we observed numerically the convergence rates of the Thomas-Fermi approximations as following: (1) in 1d: $|\mu_g - \mu_1^s| \approx O(1/\kappa_1^{0.57})$, $\|\phi_g^2 - (\phi_1^s)^2\|_{L^1} \approx O(1/\kappa_1^{0.72})$, $\|\phi_g - \phi_1^s\|_{L^2} \approx O(1/\kappa_1^{0.43})$ and $\|\phi_g - \phi_1^s\|_{L^4} \approx O(1/\kappa_1^{0.41})$ as $\frac{1}{\kappa_1} \rightarrow 0$; (2) in 2d: $|\mu_g - \mu_2^s| \approx O(1/\kappa_2^{0.40})$, $\|\phi_g^2 - (\phi_2^s)^2\|_{L^1} \approx O(1/\kappa_2^{0.58})$, $\|\phi_g - \phi_2^s\|_{L^2} \approx O(1/\kappa_2^{0.31})$ and $\|\phi_g - \phi_2^s\|_{L^4} \approx O(1/\kappa_2^{0.35})$ as $\frac{1}{\kappa_2} \rightarrow 0$; and (3) in 3d: $|\mu_g - \mu_3^s| \approx O(1/\kappa_3^{0.31})$, $\|\phi_g^2 - (\phi_3^s)^2\|_{L^1} \approx O(1/\kappa_3^{0.45})$, $\|\phi_g - \phi_3^s\|_{L^2} \approx O(1/\kappa_3^{0.24})$ and $\|\phi_g - \phi_3^s\|_{L^4} \approx O(1/\kappa_3^{0.32})$ as $\frac{1}{\kappa_3} \rightarrow 0$.

6.3 Results in 3d with cylindrical symmetry

The interesting properties of the condensation wave function in this case are its root mean square (rms) sizes in r - and z -direction r_{rms} and z_{rms} , respectively, defined by

$$r_{\text{rms}}^2 = \langle r^2 \rangle = 4\pi \int_0^\infty \int_0^\infty r^2 \psi^2(r) r dr dz, \quad (6.2)$$

$$z_{\text{rms}}^2 = \langle z^2 \rangle = 4\pi \int_0^\infty \int_0^\infty z^2 \psi^2(r) r dr dz. \quad (6.3)$$

We present computations for two cases:

		$\frac{1}{\kappa_1}$	$\frac{1}{100}$	$\frac{1}{200}$	$\frac{1}{400}$	$\frac{1}{800}$	$\frac{1}{1600}$
$ \mu_g - \mu_1^s $	Error Rate		1.875E-2 0.5655	1.267E-2 0.5711	8.528E-3 0.5775	5.715E-3 0.5827	3.816E-3
$\ \phi_g^2 - (\phi_1^s)^2\ _{L^1}$	Error Rate		9.915E-3 0.7738	5.799E-3 0.7488	3.451E-3 0.7151	2.102E-3 0.6723	1.319E-3
$\ \phi_g - \phi_1^s\ _{L^2}$	Error Rate		5.709E-2 0.4346	4.224E-2 0.4371	3.120E-2 0.4368	2.305E-2 0.4375	1.702E-2
$\ \phi_g - \phi_1^s\ _{L^4}$	Error Rate		5.676E-2 0.4079	4.278E-2 0.4103	3.219E-2 0.4080	2.426E-2 0.4083	1.828E-2

Table 5. Convergence rates of the Thomas-Femi approximations as $\frac{1}{\kappa_1} \rightarrow 0$ in 1d ($d = 1$).

		$\frac{1}{\kappa_2}$	$\frac{1}{200}$	$\frac{1}{400}$	$\frac{1}{800}$	$\frac{1}{1600}$	$\frac{1}{3200}$
$ \mu_g - \mu_2^s $	Error Rate		9.004E-2 0.3947	6.849E-2 0.4007	5.188E-2 0.4062	3.915E-2 0.4112	2.944E-2
$\ \phi_g^2 - (\phi_2^s)^2\ _{L^1}$	Error Rate		4.458E-2 0.5835	2.975E-2 0.5881	1.979E-2 0.5941	1.311E-2 0.5828	8.753E-3
$\ \phi_g - \phi_2^s\ _{L^2}$	Error Rate		1.292E-1 0.3158	1.038E-1 0.3164	8.336E-2 0.3182	6.686E-2 0.3211	5.352E-2
$\ \phi_g - \phi_2^s\ _{L^4}$	Error Rate		6.613E-2 0.3554	5.169E-2 0.3570	4.036E-2 0.3580	3.149E-2 0.3627	2.449E-2

Table 6. Convergence rates of the Thomas-Femi approximations as $\frac{1}{\kappa_2} \rightarrow 0$ in 2d ($d = 2$).

	$\frac{1}{\kappa_3}$	$\frac{1}{400}$	$\frac{1}{800}$	$\frac{1}{1600}$	$\frac{1}{3200}$	$\frac{1}{6400}$
$ \mu_g - \mu_3^s $	Error Rate	2.169E-1 0.3023	1.759E-1 0.3058	1.423E-1 0.3111	1.147E-1 0.3142	9.225E-2
$\ \phi_g^2 - (\phi_3^s)^2\ _{L^1}$	Error Rate	1.054E-1 0.4470	7.732E-2 0.4541	5.644E-2 0.4579	4.109E-2 0.4649	2.977E-2
$\ \phi_g - \phi_3^s\ _{L^2}$	Error Rate	2.046E-1 0.2437	1.728E-1 0.2461	1.457E-1 0.2455	1.229E-1 0.2492	1.034E-1
$\ \phi_g - \phi_3^s\ _{L^4}$	Error Rate	6.524E-2 0.3195	5.228E-2 0.3241	4.176E-2 0.3240	3.336E-2 0.3305	2.653E-2

Table 7. Convergence rates of the Thomas-Fermi approximations as $\frac{1}{\kappa_3} = \frac{1}{\kappa} \rightarrow 0$ in 3d ($d = 3$).

Case I. ^{87}Rb used in JILA with $\omega_x = \omega_y < \omega_z$ [7]. The detailed data are

$$m = 1.44 \times 10^{-25}[\text{kg}], \quad \omega_x = \omega_y = 20\pi[1/\text{s}], \quad \omega_z = 4\omega_x[1/\text{s}],$$

$$a_0 = \sqrt{\frac{\hbar}{\omega_x m}} = 0.3407 \times 10^{-5}[\text{m}], \quad |a| = 5.1[\text{nm}], \quad \kappa = 4\pi a N / a_0 = 0.01881N.$$

Case II. ^{23}Na used in MIT (group of Ketterle) with $\omega_x = \omega_y \gg \omega_z$ [8]. The detailed data are

$$m = 3.8 \times 10^{-26}[\text{kg}], \quad \omega_x = \omega_y = 720\pi[1/\text{s}], \quad \omega_z = 7\pi[1/\text{s}],$$

$$a_0 = \sqrt{\frac{\hbar}{\omega_z m}} = 1.1209 \times 10^{-5}[\text{m}], \quad |a| = 2.75[\text{nm}], \quad \kappa = 4\pi a N / a_0 = 0.003083N.$$

In case II, we choose $a_0 = \sqrt{\frac{\hbar}{\omega_z m}}$ (instead of $a_0 = \sqrt{\frac{\hbar}{\omega_x m}}$) as $\omega_z \ll \omega_x$ such that the root mean square size is of $O(1)$. The other parameters should be adjusted accordingly.

Figure 4 shows the ground-state condensate wave function along r - and z -axis, $\phi_g(r, 0)$ and $\phi_g(0, z)$, respectively, for different κ and surface plots of $\phi_g(r, z)$ for $\kappa = 15408$ and $\kappa = 188.1$, and Table 8 lists μ_g , $\phi_g(0, 0)$, r_{rms} , z_{rms} versus $\kappa_3 = \kappa$ for case I. Figure 5 and Table 9 show similar results for case II. Furthermore Figure 6

a	N	κ	$\phi_g(0, 0)$	r_{rms}	z_{rms}	μ_g Numerical	TFA
-5.1[nm]	250	-4.705	0.9926	0.7468	0.3268	1.9294	NA
-5.1[nm]	100	-1.881	0.6788	0.9324	0.3476	2.7283	NA
5.1[nm]	0	0	0.602	1.000	0.3539	3.000	NA
5.1[nm]	1 000	18.81	0.3824	1.325	0.3807	4.362	3.022
5.1[nm]	5 000	94.05	0.2477	1.7742	0.4214	6.680	5.752
5.1[nm]	10 000	188.1	0.2023	2.041	0.4497	8.367	7.591
5.1[nm]	50 000	940.5	0.1248	2.842	0.5532	14.95	14.45
5.1[nm]	100 000	1881	0.1012	3.276	0.6174	19.47	19.06
5.1[nm]	400 000	7524	0.0666	4.341	0.7881	33.47	33.19
5.1[nm]	800 000	15048	0.0540	4.992	8976	44.02	43.80

Table 8. Ground state chemical potential μ_g , maximum value of the wave function $\phi_g(0, 0)$ and root mean square sizes r_{rms} , z_{rms} versus the interaction coefficient $\kappa_3 = \kappa$ in 3d with cylindrical symmetry under case I.

a	N	κ	$\phi_g(0, 0)$	r_{rms}	z_{rms}	μ_g Numerical	TFA
2.75[nm]	0	0	4.3171	0.0986	0.7077	103.41	NA
2.75[nm]	1 00	0.3083	3.4797	0.0990	0.9842	104.93	NA
2.75[nm]	1 000	3.083	2.3688	0.1003	1.8842	111.71	NA
2.75[nm]	5 000	15.415	1.7450	0.1034	3.1169	127.69	NA
2.75[nm]	10 000	30.83	1.5082	0.1061	3.8457	141.13	86.11
2.75[nm]	50 000	154.15	1.0202	0.1179	6.0508	202.04	163.9
2.75[nm]	100 000	308.3	0.8416	0.1267	7.2226	248.1	216.3
2.75[nm]	500 000	1541.5	0.5215	0.1588	10.501	432.06	411.80
2.75[nm]	1 000 000	3083	0.4226	0.1784	12.203	559.92	543.37
2.75[nm]	5 000 000	15415	0.2598	0.2396	17.070	1044.7	1034.4

Table 9. Ground state chemical potential μ_g , maximum value of the wave function $\phi_g(0, 0)$ and root mean square sizes r_{rms} , z_{rms} versus the interaction coefficient $\kappa_3 = \kappa$ in 3d with cylindrical symmetry under case II.

compares the numerical ground state solution (i.e. numerical solution of (5.9)) and the Thomas-Fermi approximation (TFA) in (5.18).

From Figures 4-5, and Tables 8-9, we can see that the chemical potential μ_g and the root mean square sizes r_{rms} , z_{rms} will increase when the interaction coefficient $\kappa_3 = \kappa$ (i.e. the number of atoms in the condensate) is increasing. On the other hand, the peak of the ground state solution $\phi_g(0,0)$ will decrease. Figure 6 and Table 8-9 show that the Thomas-Fermi approximation are accurate for the chemical potential and ground state wave function near the origin only when κ is very big, but gives poor approximation when κ is intermediate or in the tail of the wave function.

6.4 Application to compute excited states of GPE

Suppose the eigenfunctions of the nonlinear eigenvalue problem (3.2) under the constraint (3.3) are

$$\pm\phi_g(\mathbf{x}), \pm\phi_1(\mathbf{x}), \pm\phi_2(\mathbf{x}), \dots,$$

whose energies satisfy

$$E_\kappa(\phi_g) < E_\kappa(\phi_1) < E_\kappa(\phi_2) < \dots.$$

Then ϕ_j is called as the j -th excited state solution of the GPE (2.13). In fact, ϕ_g and ϕ_j ($j = 1, 2, \dots$) are critical points of the energy functional $E_\kappa(\phi)$ under the constraint (3.3). In 1d, when $V(x) = \frac{x^2}{2}$ is chosen as the harmonic oscillator potential and $\kappa_1 = 0$, the excited states are given [33]:

$$\begin{aligned} \phi_j(x) &= \left(2^j j!\right)^{-1/2} \left(\frac{1}{\pi}\right)^{1/4} e^{-x^2/2} H_j(x), \\ \mu_j = \mu_0(\phi_j) = E_0(\phi_j) &= \left(j + \frac{1}{2}\right), \quad j = 1, 2, \dots; \end{aligned}$$

where $H_j(x)$ is the standard j -th Hermite function [33]. Here we show numerically that the algorithm (3.9) can also be applied to compute any j -th excited state of GPE with $\kappa_1 > 0$ provided that we start with the above j -th excited state as initial data for $\kappa_1 > 0$ small and use a continuation technique for $\kappa_1 > 0$ bigger, i.e. use the numerical solution of the j -th excited state solution for a small κ_1 as initial guess for computing the j -th excited state of a larger κ_1 . When the algorithm (3.9) is applied to compute j -th (j is an odd integer) excited state in 1d, due to these functions are odd function, the finite element subspace in Section 4 should be replaced by

$$\begin{aligned} \tilde{V}_g^h &= \left\{ \phi^h(r) \in C([0, R]) \mid \phi^h(r)|_{[r_j, r_{j+1}]} \in P_1([r_j, r_{j+1}]), \quad 0 \leq j \leq M-1, \right. \\ &\quad \left. \phi^h(0) = \phi^h(R) = 0 \right\}. \end{aligned}$$

For simplicity, here we only report numerical results in 1d for the first four excited states of GPE for different $\kappa_1 \geq 0$. Table 10 shows the energy $E_\kappa(\phi_j)$ and chemical

κ_1	0	3.1371	12.5484	31.371	62.742	156.855	313.71
$E_\kappa(\phi_g)$	0.5000	1.0441	2.2330	3.9810	6.2569	11.464	18.171
$E_\kappa(\phi_1)$	1.5000	1.9414	3.0377	4.7438	6.9998	12.191	18.891
$E_\kappa(\phi_2)$	2.5000	2.8865	3.9039	5.5573	7.7824	12.944	19.629
$E_\kappa(\phi_3)$	3.5000	3.8505	4.8038	6.4043	8.5938	13.719	20.383
$E_\kappa(\phi_4)$	4.5000	4.8245	5.7252	7.2752	9.4276	14.511	21.150
μ_g	0.5000	1.5266	3.5966	6.5527	10.369	19.070	30.259
μ_1	1.5000	2.3578	4.3442	7.2802	11.089	19.784	30.971
μ_2	2.5000	3.2590	5.1479	8.0432	11.833	20.512	31.691
μ_3	3.5000	4.1919	5.9901	8.8349	12.597	21.252	32.419
μ_4	4.5000	5.1424	6.8598	9.6501	13.381	22.005	33.157

Table 10. Energy and chemical potential of the ground state and first four excited states of GPE in 1d ($d = 1$).

potential μ_j ($j = g, 1, 2, 3, 4$) of the ground state and first four excited states of GPE in 1d for different κ_1 . Figure 7 plots the first four excited wave functions $\phi_j(x)$ ($j = 1, 2, 3, 4$) versus x for different κ_1 .

From the results in Table 10 and Figure 7, we can see that the algorithm (3.9) can be applied to compute the excited states of GPE (2.13). We observed from our numerical results in Table 10 that for any fixed $\kappa_1 \geq 0$

$$E_\kappa(\phi_g) < E_\kappa(\phi_1) < E_\kappa(\phi_2) < \cdots, \quad \mu_g < \mu_1 < \mu_2 < \cdots.$$

This implies that the eigenvalue of (3.2), μ_g , corresponding to the minimizer of the energy functional $E_\kappa(\phi)$, ϕ_g , is the minimum chemical potential among all the eigenvalues of (3.2). Furthermore, we have

$$\lim_{\kappa_1 \rightarrow +\infty} \frac{E_\kappa(\phi_j)}{E_\kappa(\phi_g)} = 1, \quad \lim_{\kappa_1 \rightarrow +\infty} \frac{\mu_j}{\mu_g} = 1, \quad j = 1, 2, 3, 4.$$

A rigorous mathematical justification of these numerical observations is under further study.

7 Conclusions

Ground state solution of time-independent Gross-Pitaevskii equation of Bose-Einstein condensation at zero or very low temperature is computed by directly minimizing the energy functional under a constraint through the finite element discretization. We begin with the 3d Gross-Pitaevskii equation, scale it to obtain a three-parameter model, show how to reduce it to 2d and 1d GPEs. The ground state solution is formulated via minimizing the energy functional under a constraint. The finite element

approximation for 1d, 2d with radial symmetry and 3d with spherical symmetry and cylindrical symmetry are presented in detail and approximate ground state solutions, which are used as initial guess in our practical numerical computation, are provided in two extreme regimes: very weak interactions and strong repulsive interactions. Numerical results are reported in 1d, 2d with radial symmetry and 3d with spherical symmetry and cylindrical symmetry for condensation with repulsive/attractive interparticle interactions and atoms in it ranging up to millions to demonstrate the novel numerical method. Our numerical results show that the Thomas-Fermi approximation are accurate for the chemical potential and ground state wave function near the origin only when κ is very big, but gives poor approximation when κ is intermediate or in the tail of the wave function. Furthermore extension of our method to compute the excited states of GPE is also presented. In the future we plan to study physically more complex systems based on this ground state solution solver.

Acknowledgment

W.B. acknowledges support by the National University of Singapore grant No. R-151-000-027-112 and helpful discussion with Peter A. Markowich. W. T. acknowledges support by the National University of Singapore, hospitality by Guowei Wei and Yingfei Yi for his extended visit at Department of Computational Science, National University of Singapore, and support by the National Natural Science Foundation of China grant No. 19901004-1. The authors thank the referees for their very helpful suggestions and comments to improve the paper.

References

- [1] R. A. Adams, Sobolev Spaces, 1975.
- [2] S.K. Adhikari, Numerical solution of the two-dimensional Gross-Pitaevskii equation for trapped interacting atoms, Phys. Lett. A 265, 91 (2000).
- [3] S.K. Adhikari, Numerically study of the spherically symmetric Gross-Pitaevskii equation in two space dimensions, Phys. Rev. E 62, 2937 (2000).
- [4] S.K. Adhikari, Collapse of attractive Bose-Einstein condensed vortex states in a cylindrical trap, Phys. Rev. E 65, 016703 (2002).
- [5] S.K. Adhikari and P. Muruganandam, Bose-Einstein condensation dynamics from the numerical solution of the Gross-Pitaevskii equation, J. Phys. B 35, 2831 (2002).
- [6] A. Aftalion A, and Q. Du, Vortices in a rotating Bose-Einstein condensate: Critical angular velocities and energy diagrams in the Thomas-Fermi regime, Phys. Rev. A 64, 063603 (2001).

- [7] M.H. Anderson, J.R. Ensher, M.R. Mathews, C.E. Wieman and E.A. Cornell, *Science* 269, 198 (1995).
- [8] J.R. Anglin and W. Ketterle, Bose-Einstein condensation of atomic gases, *Nature* 416, 211 (2002).
- [9] W. Bao, D. Jaksch and P.A. Markowich, Numerical solution of the Gross-Pitaevskii equation for Bose-Einstein condensation, *J. Comput. Phys.*, in press.
- [10] W. Bao, Shi Jin and P.A. Markowich, On time-splitting spectral approximations for the Schrödinger equation in the semiclassical regime, *J. Comput. Phys.* 175, 487 (2002).
- [11] W. Bao, Shi Jin and P.A. Markowich, Numerical study of time-splitting spectral discretizations of nonlinear Schrödinger equations in the semi-classical regimes, *SIAM J. Sci. Comput.*, to appear.
- [12] S.N. Bose, *Z. Phys.* 26, 178 (1924).
- [13] C.C. Bradley, C.A. Sackett, R.G. Hulet, *Phys. Rev. Lett.* 78, 985 (1997).
- [14] M.M. Cerimele, M.L. Chiofalo, F. Pistella, S. Succi and M.P. Tosi, Numerical solution of the Gross-Pitaevskii equation using an explicit finite-difference scheme: An application to trapped Bose-Einstein condensates, *Phys. Rev. E* 62, 1382 (2000).
- [15] M.M. Cerimele, F. Pistella and S. Succi, Particle-inspired scheme for the Gross-Pitaevskii equation: An application to Bose-Einstein condensation, *Comput. Phys. Comm.* 129, 82 (2000).
- [16] M.L. Chiofalo, S. Succi and M.P. Tosi, Ground state of trapped interacting Bose-Einstein condensates by an explicit imaginary-time algorithm, *Phys. Rev. E* 62, 7438 (2000).
- [17] P.G. Ciarlet, *The Finite Element Method for Elliptic Problems* (North-Holland, 1978).
- [18] E. Cornell, Very cold indeed: The nanokelvin physics of Bose-Einstein condensation, *J. Res. Natl. Inst. Stan.* 101, 419 (1996).
- [19] F. Dalfovo and S. Stringari, Bosons in anisotropic traps: Ground state and vortices, *Phys. Rev. A* 53, 2477 (1996).
- [20] R.J. Dodd, Approximate solutions of the nonlinear Schrödinger equation for ground and excited states of Bose-Einstein condensates, *J. Res. Natl. Inst. Stan.* 101, 545 (1996).

- [21] M. Edwards and K. Burnett, Numerical solution of the nonlinear Schrödinger equation for small samples of trapped neutral atoms, *Phys. Rev. A* 51, 1382 (1995).
- [22] A. Einstein, *Sitz. Ber. Kgl. Preuss. Adad. Wiss.* 22, 261 (1924).
- [23] J.R. Ensher, D.S. Jin, M.R. Mathews and C.E. Wieman and E.A. Cornell, *Phys. Rev. Lett.* 77, 4984 (1996).
- [24] A. Gammal, T. Frederico and L. Tomio, Improved numerical approach for the time-independent Gross-Pitaevskii nonlinear Schrödinger equation, *Phys. Rev. E* 60, 2421 (1999).
- [25] A. Griffin, D. Snoke, S. Stringaro (Eds.), *Bose-Einstein condensation* (Cambridge University Press, New York, 1995).
- [26] D. Gottlieb and S.A. Orszag, *Numerical Analysis of Spectral Methods* (Soc. for Indust. & Appl. Math., Philadelphia, 1977).
- [27] E.P. Gross, *Nuovo. Cimento.* 20, 454 (1961).
- [28] M.J. Holland, D.S. Jin, M.L. Chiofalo and J. Cooper, Emergence of interaction effects in Bose-Einstein condensation, *Phys. Rev. Lett.* 78, 3801 (1997).
- [29] A.D. Jackson, G.M. Kavoulakis and C.J. Pethick, Solitary waves in clouds of Bose-Einstein condensed atoms, *Phys. Rev. A* 58, 2417 (1998).
- [30] L. Landau and E. Lifschitz, *Quantum Mechanics: non-relativistic theory* (Pergamon Press, New York, 1977).
- [31] P. Leboeuf and N. Pavloff, *Phys. Rev. A* 64, 033602 (2001); V. Dunjko, V. Lorent, and M. Olshanii, *Phys. Rev. Lett.* 86, 5413 (2001).
- [32] E.H. Lieb, R. Seiringer and J. Yngvason, Bosons in a Trap: A Rigorous Derivation of the Gross-Pitaevskii Energy Functional, *Phys. Rev. A* 61, 3602 (2000).
- [33] I. N. Levine, *Quantum Chemistry (Fifth Edition)* (Prentice Hall International, Inc., New York, 1991).
- [34] K. W. Morton and D. F. Mayers, *Numerical Solution of Partial Differential Equations* (Cambridge University Press, 1994).
- [35] S. G. Nash and A. Sofer, *Linear and nonlinear programming* (McGraw-Hill, New York, 1996).
- [36] L.P. Pitaevskii, *Zh. Eksp. Teor. Fiz.* 40, 646 (1961). (*Sov. Phys. JETP* 13, 451 (1961)).

- [37] P.A. Ruprecht, M.J. Holland, K. Burrett and M. Edwards, Time-dependent solution of the nonlinear Schrödinger equation for Bose-condensed trapped neutral atoms, *Phys. Rev. A* 51, 4704 (1995).
- [38] B.I. Schneider and D.L. Feder, Numerical approach to the ground and excited states of a Bose-Einstein condensated gas confined in a completely anisotropic trap, *Phys. Rev. A* 59, 2232 (1999).

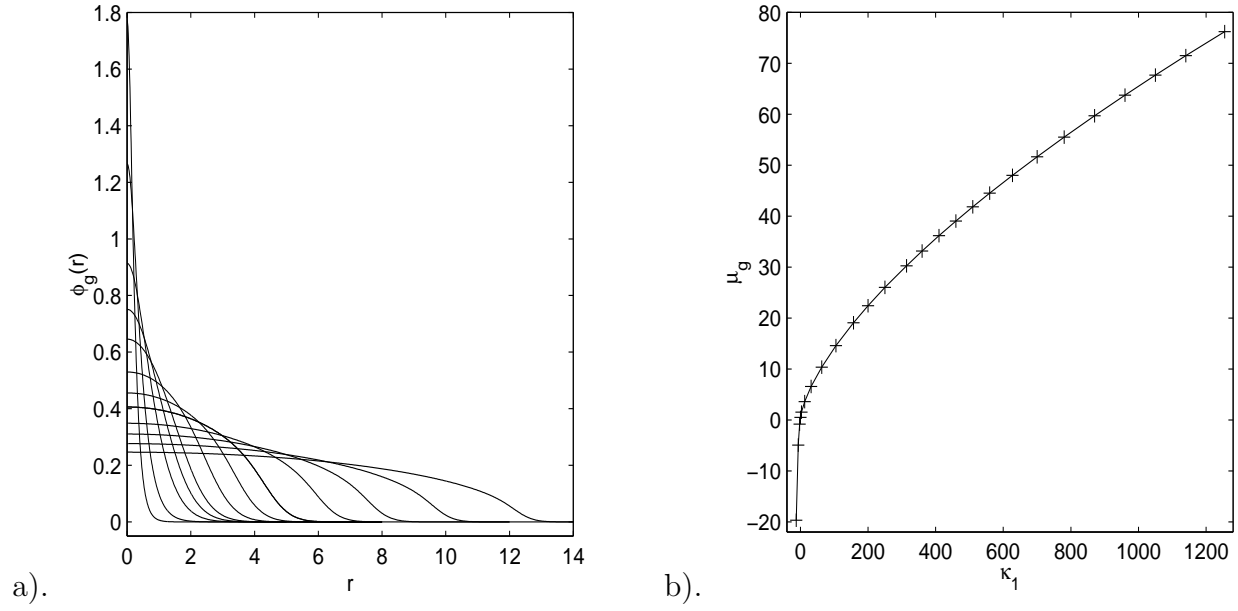


Figure 1: Ground-state condensate solution in 1d ($d = 1$). a). Wave function $\phi_g(r)$ versus r for $\kappa_1 = -12.5484, -6.2742, -2.5097, 0, 3.1371, 12.5484, 31.371, 62.742, 156.855, 313.71, 627.42, 1254.8$ (in order of increasing width). b). Chemical potential μ_g versus κ_d .

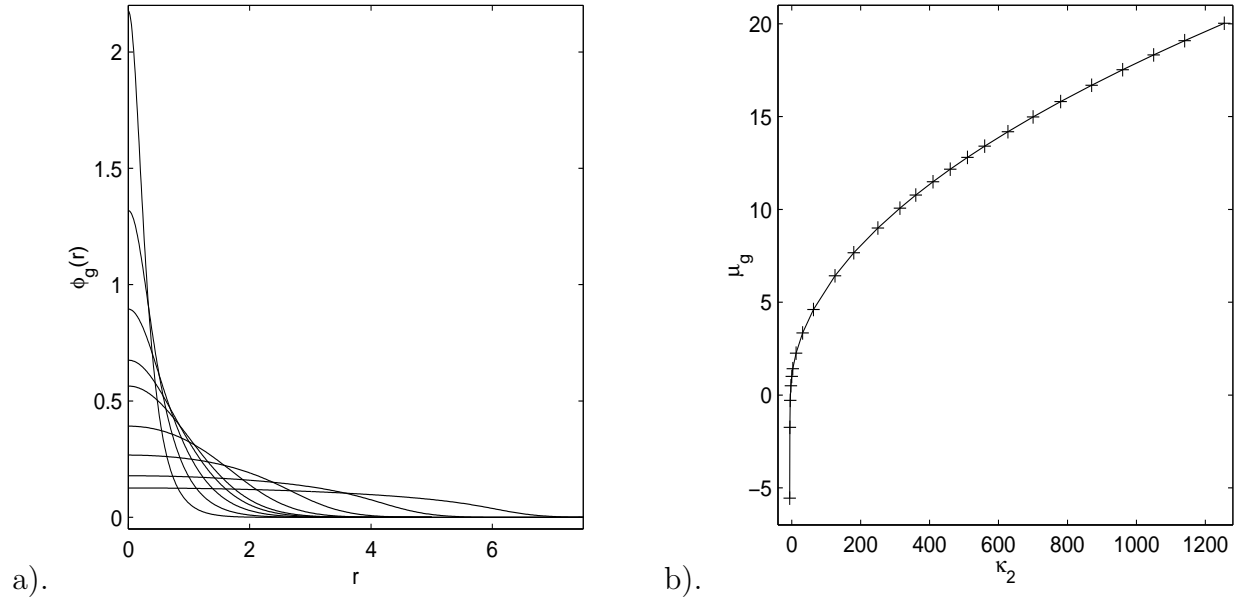


Figure 2: Ground-state condensate solution in 2d with radial symmetry. a). Wave function $\phi_g(r)$ versus r for $\kappa_2 = -5.8, -5.5, -4.5, -2.5097, 0, 12.5484, 62.742, 313.71, 1254.8$ (in order of increasing width). b). Chemical potential μ_g versus κ_d .

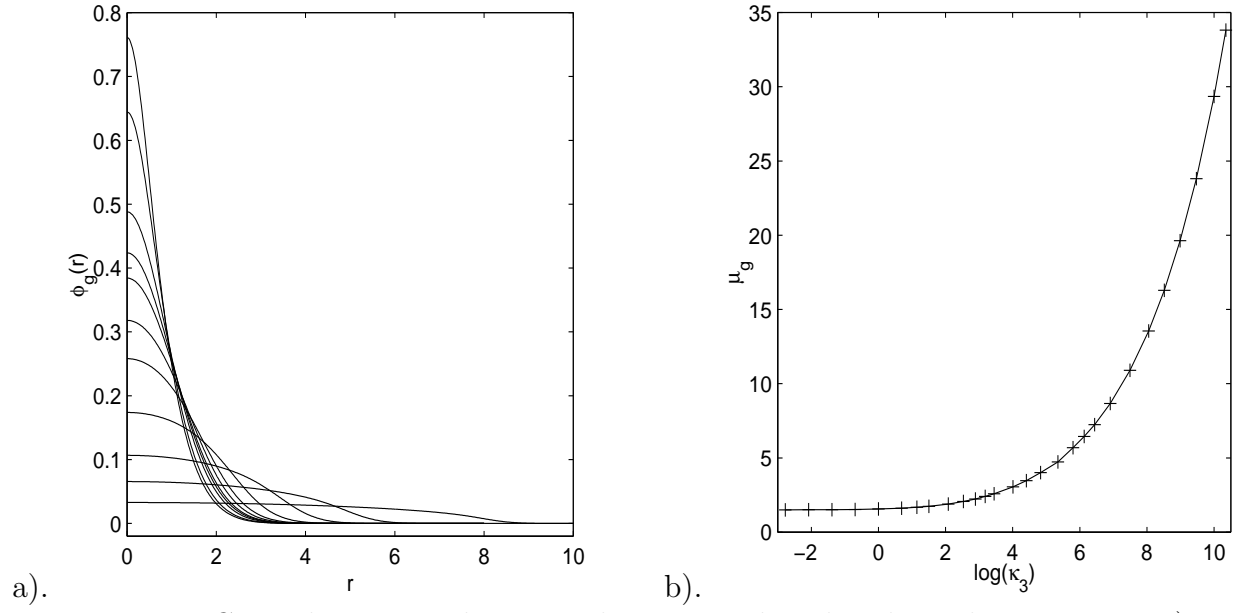


Figure 3: Ground-state condensate solution in 3d with spherical symmetry. a). Wave function $\phi_g(r)$ versus r for $\kappa_3 = -7, -6.2472, -3.1371, 0, 3.1371, 12.5484, 31.371, 125.484, 627.42, 3137.1, 31371$ (in order of increasing width). b). Chemical potential μ_g versus κ_d .

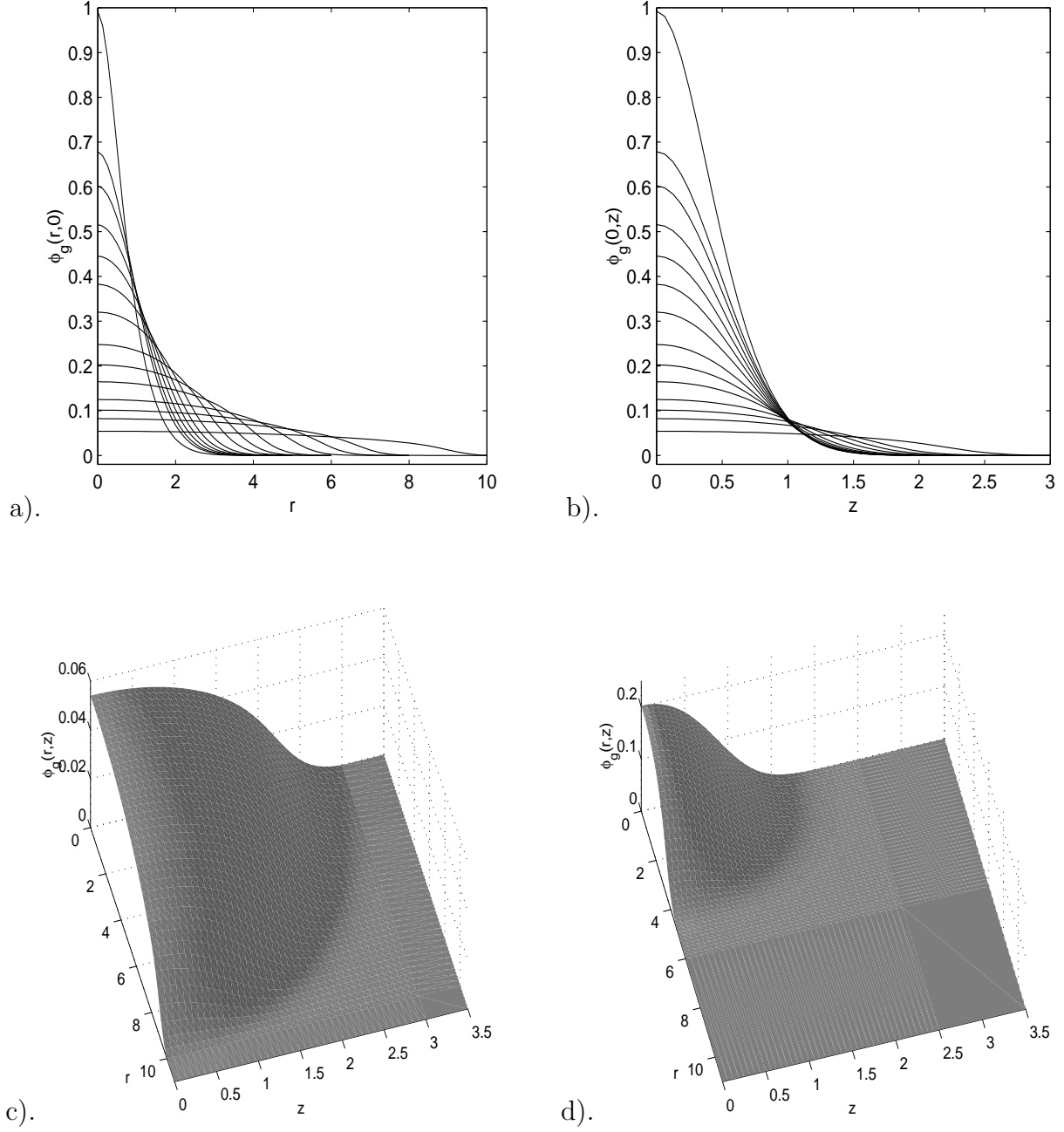


Figure 4: Ground-state solution in 3d with cylindrical symmetry under case I. Condensate wave function on two lines for $\kappa_3 = -4.705, -1.881, 0, 3.762, 9.405, 18.81, 37.62, 94.05, 188.1, 376.2, 940.5, 1881, 3762$ and 15048 (in order of increasing width): a). On the line $z = 0$ ($\phi_g(r, 0)$); b). On the line $r = 0$ ($\phi_g(0, z)$). Surface Plots of the condensate wave function $\phi_g(r, z)$: c). $\kappa_3 = 15048$ ($N = 800\,000$); d). $\kappa_3 = 188.1$ ($N = 10\,000$).

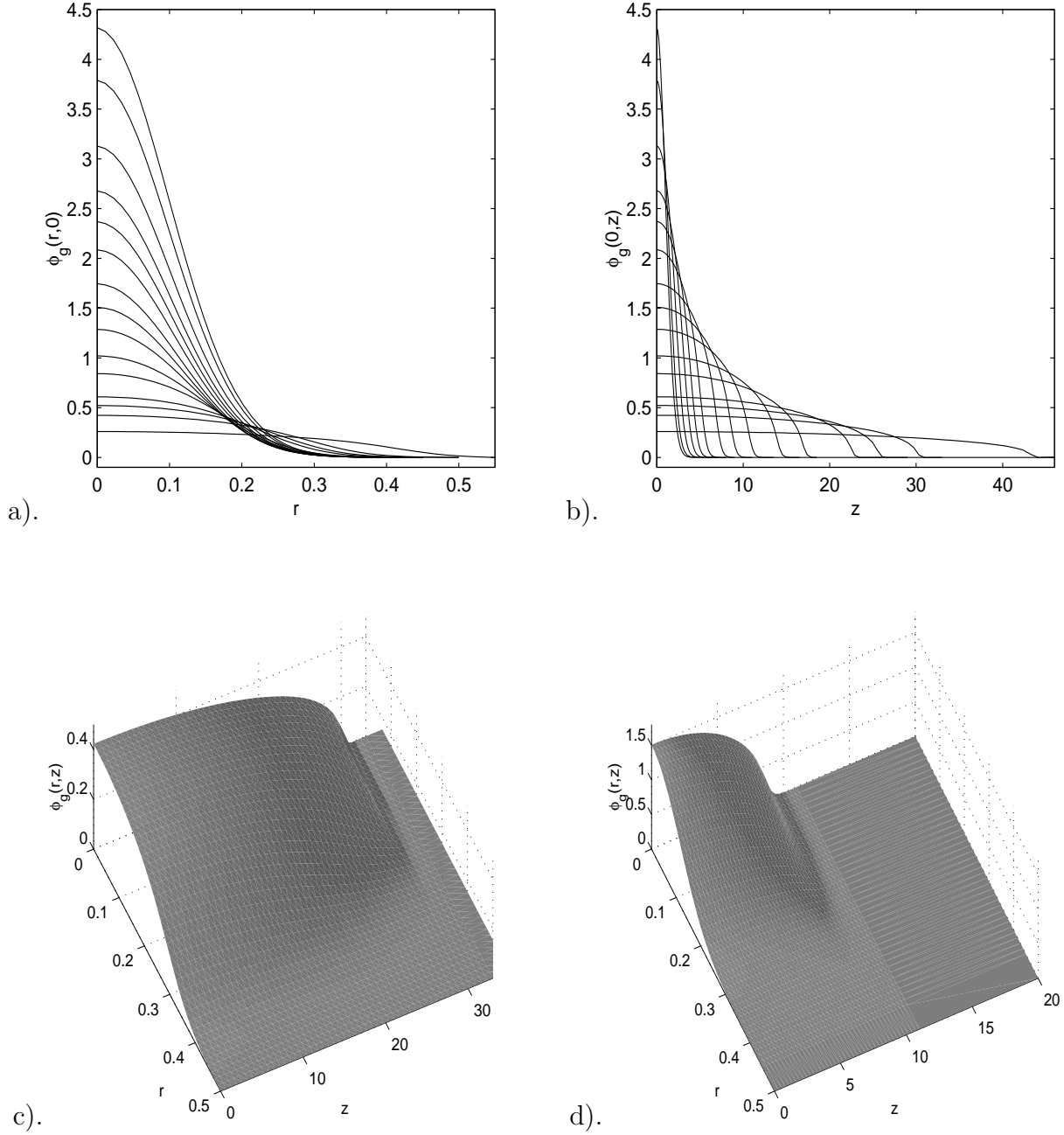


Figure 5: Ground-state solution in 3d with cylindrical symmetry under case II. Condensate wave function on two lines for $\kappa_3 = 0, 0.15415, 0.6166, 1.5415, 3.083, 6.166, 15.415, 30.83, 61.66, 154.15, 308.3, 924.9, 1541, 3083$ and 15415 (in order of increasing width): a). On the line $z = 0$ ($\phi_g(r, 0)$); b). On the line $r = 0$ ($\phi_g(0, z)$). Surface Plots of the condensate wave function $\phi_g(r, z)$: c). $\kappa_3 = 3083$ ($N = 1\,000\,000$); d). $\kappa_3 = 30.83$ ($N = 10\,000$).

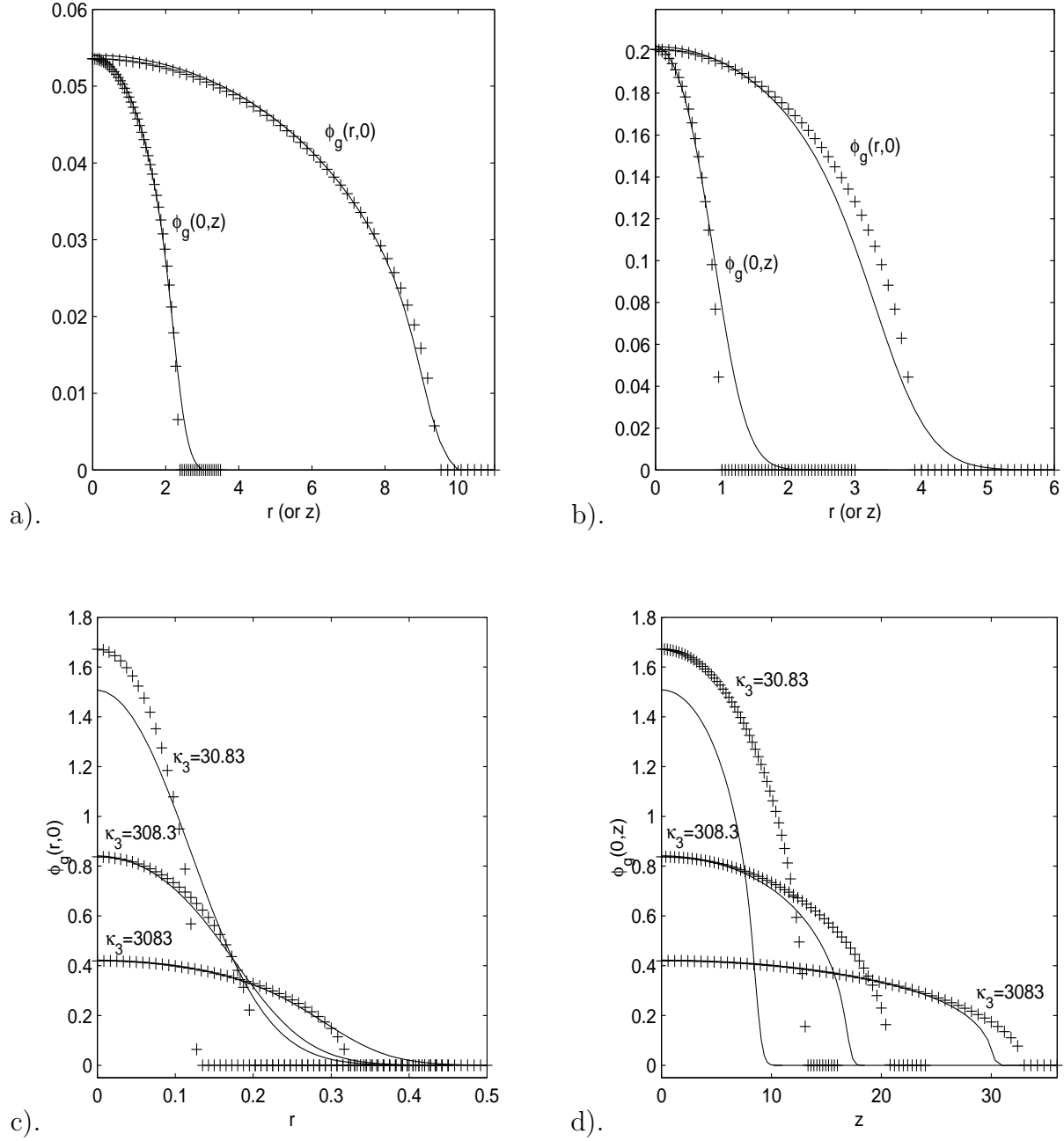


Figure 6: Comparison between the numerical ground state solution and the Thomas-Fermi approximation in 3d with cylindrical symmetry. ‘—’: Numerical solution of (5.9), ‘+ + +’: Thomas-Fermi approximation (5.18). For case I: a). $\kappa_3 = 15048$ ($N = 800\,000$); b). $\kappa_3 = 188.1$ ($N = 10\,000$). For case II: c). At the line $z = 0$, i.e. $\phi_g(r, 0)$; d). At the line $r = 0$, i.e. $\phi(0, z)$.

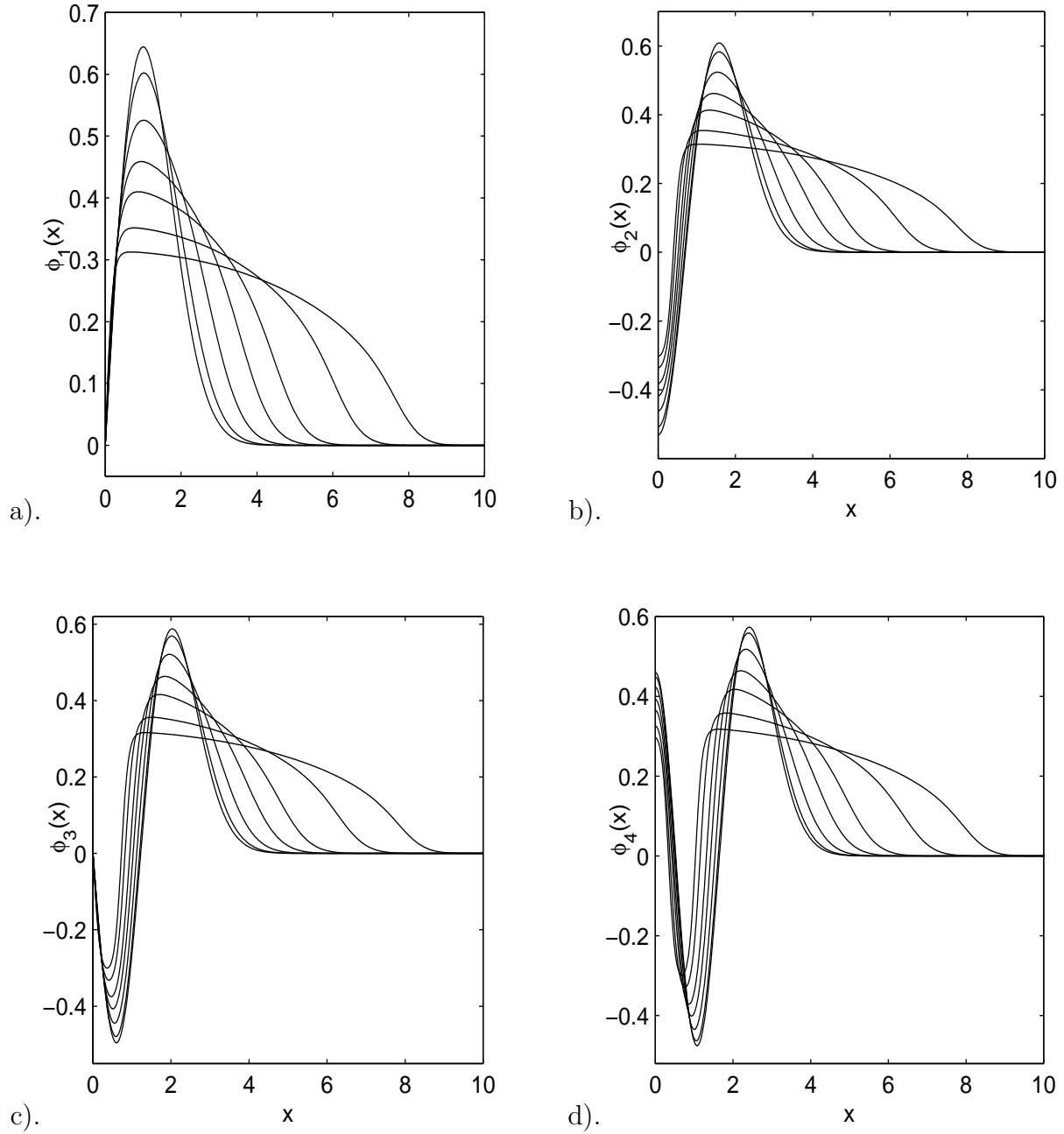


Figure 7: Excited states of GPE with harmonic oscillator potential in 1d for $\kappa_1 = 0, 3.1371, 12.5484, 31.371, 62.742, 156.855, 313.71$ (in order of increasing width). a). First excited state $\phi_1(x)$ (odd function); b). Second excited state $\phi_2(x)$ (even function); c). Third excited state $\phi_3(x)$ (odd function); d). Fourth excited state $\phi_4(x)$ (even function).